Journal of the Iranian Chemical Society (2023) 20:109–123
https://doi.org/10.1007/s13738-022-02659-9

ORIGINAL PAPER

Crystal structure, Hirshfeld surface analysis, computational and antifungal studies of dihydropyrimidines on the basis of salicylaldehyde derivatives

Alakbar Huseynzada[1,8,10] · Christian Jelsch[2] · Haji Vahid Akhundzada[1,3,8] · Sarra Soudani[4] · Cherif Ben Nasr[4] · Koray Sayin[5] · Mustafa Demiralp[6] · Ulviyya Hasanova[1,8] · Goncha Eyvazova[7] · Zarema Gakhramanova[8] · Vagif Abbasov[9]

Received: 29 January 2022 / Accepted: 30 August 2022 / Published online: 13 September 2022

Abstract

We herein reported the synthesis of dihydropyrimidines **1** and **2** on the basis of nitro and brominated salicylaldehyde derivatives by Biginelli reaction in microwave conditions in the presence of cheap low toxic copper triflate. The structures of both compounds were investigated by the X-ray single-crystal diffraction method. The presence of non-covalent interactions and their impact on crystal structure was determined. In addition, the conformation of the dihydropyrimidine ring was also studied. In order to understand the molecular interactions in their structure, the Hirshfeld surface and contacts enrichment analyses were performed. Moreover, the biological activity of synthesized compounds was also investigated against *Candida albicans* and *Aspergillus niger* fungi. Finally, computational studies of the related compounds were performed at M062X/6-31G(d) level in the water and molecular docking calculations were done against the thymidylate kinase of *Candida albicans*.

Keywords Microwave-assisted synthesis · Biginelli reaction · Conformation analysis · Hirshfeld surface analysis · Non-covalent interactions · Molecular docking

Introduction

The one-pot multicomponent reaction between aldehyde, urea derivative and methylene active compound, which leads to the synthesis of two nitrogen atoms containing six-membered heterocycles, viz., dihydropyrimidines, was discovered by Italian chemist Pietro Biginelli in 1893 [1]. Even though from the year of discovering more than 100 years past, it still keeps its actuality due to the wide spectrum of biological activities of its reaction products [2]. Variation of all three building blocks allowing introducing various pharmacophoric groups leads to the large molecular diversity of dihydropyrimidines, which biological activity studies reveal such activities as antiviral [3, 4], antiproliferative [5, 6], antitumor [7–12], antibacterial [13–19], anti-inflammatory [20–22], antitubercular [23], antifungal [24], antileishmanial [25], anti-hypertensive [26–28], antiepileptic [29], antidiabetic [30, 31], anti-HIV [32], antimalarial [33],

✉ Alakbar Huseynzada
alakbar.huseynzada1117@gmail.com

1 Baku State University, ICRL, Z. Khalilov 23, Baku AZ 1148, Azerbaijan

2 Université de Lorraine, CNRS, CRM2, 54000 Nancy, France

3 Institute of Radiation Problems of ANAS, B. Vahabzada 9, Baku AZ 1143, Azerbaijan

4 Laboratoire de Chimie des Matériaux, Faculté des Sciences de Bizerte, Université de Carthage, 7021 Zarzouna, Tunisia

5 Chemistry Department, Sivas Cumhuriyet University, Sivas, Turkey

6 LC-MS Laboratory, Advanced Technology Research and Application Center, Sivas Cumhuriyet University, Sivas, Turkey

7 Nanoresearch Center, Baku State University, Z. Khalilov 23, Baku AZ 1148, Azerbaijan

8 Geotechnological Problems of Oil, Gas and Chemistry, Azerbaijan State Oil and Industry University, Baku, Azerbaijan

9 Institute of Petrochemical Processes, K. Avenue 30, Baku AZ 1005, Azerbaijan

10 Chemistry Department, Azerbaijan Engineers Union, Bashir Safaroglu 118, Baku, Azerbaijan

mPGES-1 inhibitors [34], miscellaneous [35–37] activities, as well as calcium [38] and potassium channels [39–41] and α-1A adrenergic antagonists [42]. Long and painstaking investigations of these heterocycles allowed synthesizing of different drugs on the basis of them which found application against HIV (batzelladine A and B) [32], cancer (monastrol, enastron, mon-97 and fluorastrol) [7–12], benign prostatic hyperplasia (prostate enlargement) and high blood pressure (terazosin) [36].

Considering their importance in pharmacy, their synthesis methods in the presence of building blocks with various functional groups are always modified by chemists in order to find a more benign, cheaper and "green" method. Along with synthesis methods, computational studies and crystal structure investigations of dihydropyrimidines are also very important, which provide key information about non-covalent interactions and their role in crystal packing, tautomerization and conformation of dihydropyrimidine ring [43–45] allowing delving into the structure–biological activity relationship of investigated compounds [46].

Taking into account all above mentioned, we perform a synthesis of dihydropyrimidines in the presence of low toxic copper triflate on the basis of salicylaldehyde derivatives—2-hydroxy-5-nitrobenzaldehyde and 5-bromo-2-hydroxybenzaldehyde. The structures of synthesized compounds **1** and **2** were studied by X-ray single-crystal diffraction method, which allowed studying of the conformation of the dihydropyrimidine ring and the presence of various interactions in crystal packing. In order to understand the molecular interactions in their structure, the Hirshfeld surface and contacts enrichment analyses were also performed. Considering the broad spectrum of biological activity of dihydropyrimidines, synthesized compounds **1** and **2** were studied against *Candida albicans* and *Aspergillus niger* fungi, where results were compared with the known antifungal drug fluconazole. In addition to it, computational studies at M062X/6-31G(d) level in the water and molecular docking calculations against thymidylate kinase of *Candida albicans* were also performed.

Materials and methods

General information

All the solvents and reagents were purchased from commercial suppliers and were of analytical grade and used without further purification. The control of the reactions progress and the determination of the synthesized compounds' purity were done by thin-layer chromatography (TLC) on Merck silica gel plates (60 F254 aluminium sheets) which were visualized under UV light. Melting points were recorded in open capillary tubes on a Buchi B-540 apparatus and were uncorrected. Elemental analysis was performed on the Carlo Erba 1108 analyser.

Experimental synthesis procedure

The synthesis of compounds was done according to the known procedure and NMR and mass data were compared with the literature [45].

In details, 0.5 mmol of salicylaldehyde derivative, 0.75 mmol (45 mg) of urea and 0.08 mmol (30 mg) of $Cu(OTf)_2$ were added to a microwave vial with a magnetic stirrer and dissolved in 1 ml of DMSO (Fig. 1). Subsequently, 0.46 mmol (50 µl) of methyl acetoacetate was added to a vial, which was sealed and irradiated at 100 °C in a microwave reactor for 2 h at a maximum power of 200 W (CEM Discover™ System). At the end of the reaction time, the reaction mixture was poured on ice; the precipitate was formed, filtered, washed with distilled water and dried. Further purification of compounds was done by the Biotage Isolera One Flash Chromatography System (cyclohexane-ethyl acetate–methanol).

Compound (I) methyl 4-(5-bromo-2-hydroxyphenyl)-6-methyl-2-oxo-1,2,3,4-tetrahydropyrimidine-5-carboxylate. The title compound was prepared according to the general procedure using 5-bromo-2-hydroxy-benzaldehyde to afford the title compound a yellow-green precipitate. Yield 71.5%. M.p. 215–217 °C. **^{1}H NMR** spectrum: (DMSO-d_6, δ, ppm), 2.27 s (3H, CH_3), 3.49 s (3H, OCH_3), 5.39 s (1H,

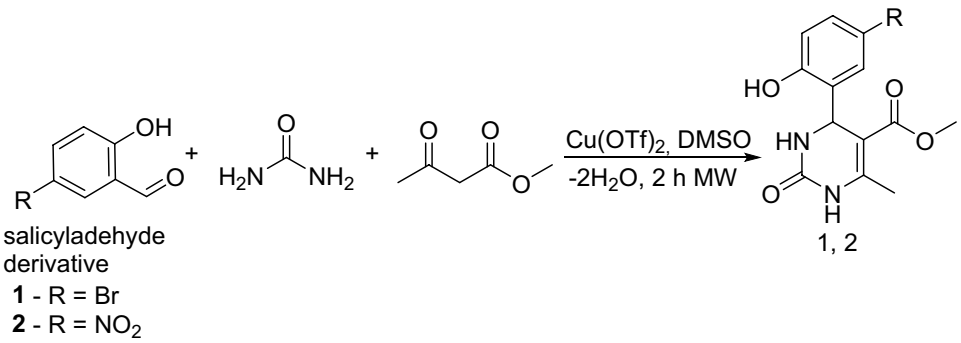

Fig. 1 Synthesis of dihydropyrimidines **1** and **2** on the basis of salicylaldehyde derivatives

CH), 6.74–6.78 d (1H, $C_{Ar}H$, J = 12 Hz), 7.0 s (1H, $C_{Ar}H$), 7.20–7.27 m (2H, $C_{Ar}H$ + NH), 9.20 s (1H, NH), 10.01 s (1H, NH). **^{13}C NMR** spectrum: (DMSO-d_6, δ, ppm), 17.76 (CH_3), 48.78 (CH), 50.7 (OCH_3), 96.99 (C), 118.01 ($C_{Ar}H$), 120.33 ($C_{Ar}H$), 121.52 ($C_{Ar}H$), 128.98 (C_{Ar}), 129.37 (C_{Ar}), 149.28 (C), 152.13 (C_{Ar}), 155.89 (COO), 165.74 (CO). HRMS (ESI-MS): 341.11 [$M^+ + H^+$] (Figure 1S, 2S, 5S). Elemental analysis calcd. for $C_{13}H_{13}N_2O_4Br$, %: C, 45.77; H, 3.84; N, 8.21. Found, %: C, 45.73; H, 3.81; N, 8.25.

Compound (2) methyl 4-(2-hydroxy-5-nitrophenyl)-6-methyl-2-oxo-1,2,3,4-tetrahydropyrimidine-5-carboxylate. The title compound was prepared according to the general procedure using 2-hydroxy-5-nitrobenzaldehyde to afford the title compound a yellow-green precipitate. Yield 79%. M.p. 239–240 °C. **^{1}H NMR** spectrum: (DMSO-d_6, δ, ppm), 2.30 s (3H, CH_3), 3.49 s (3H, OCH_3), 5.48 s (1H, CH), 6.97 s (1H, $C_{Ar}H$), 7.44 s (1H, $C_{Ar}H$), 7.87 s (1H, $C_{Ar}H$), 8.06 s (1H, NH), 9.28 s (1H, NH), 11.36 br s (1H, NH). **^{13}C NMR** spectrum: (DMSO-d_6, δ, ppm), 17.80 (CH_3), 49.38 (CH), 50.78 (OCH_3), 96.60 (C), 115.95 (C_{Ar}), 123.56 (C), 124.93 ($C_{Ar}H$), 139.25 ($C_{Ar}H$), 149.60 ($C_{Ar}H$), 151.94 ($2C_{Ar}$), 161.68 (COO), 165.63 (CO). HRMS (ESI-MS): 308.08 [$M^+ + H^+$], 330.08 [$M^+ + Na^+$], 306.08 [M^+-H^+] (Figure 3S, 4S, 6S). Elemental analysis calcd. for $C_{13}H_{13}N_3O_6$, %: C, 50.82; H, 4.26; N, 13.68. Found, %: C, 50.88; H, 4.21; N, 13.61.

NMR experiments

The NMR experiments were performed on a BRUKER FT NMR spectrometer AVANCE 300 (Bruker, Karlsruhe, Germany) (300 MHz for ^{1}H and 75 MHz for ^{13}C) with a BVT 3200 variable temperature unit in 5 mm sample tubes using Bruker Standard software (TopSpin 3.1). Chemical shifts were given in ppm (δ) and were referenced to internal tetramethylsilane (TMS). Coupling constants J are given in Hz. The experimental parameters for ^{1}H are as follows: digital resolution = 0.23 Hz, SWH = 7530 Hz, TD = 32 K, SI = 16 K, 90 pulse length = 10 ms, PL1 = 3 dB, ns = 1, ds = 1, d1 = 1 s and for ^{13}C as follows: digital resolution = 0.27 Hz, SWH = 17,985 Hz, TD = 64 K, SI = 32 K, 90 pulse length = 9 ms, PL1 = 1.5 dB, ns = 500, ds = 2, d1 = 3 s. The NMR-grade DMSO-d_6 (99.7%, containing 0.3% H_2O) was used for the solutions of synthesized compounds **1** and **2**, which are stable in the solution phase.

Mass experiments

High-resolution mass spectrometry (HRMS) was performed using electrospray ionization (ESI) in positive-ion or negative-ion detection mode.

X-Ray analysis

X-Ray analyses were performed on Bruker SMART APEX II single-crystal X-ray diffractometer equipped with graphite-monochromated Mo-Kα radiation (λ = 0.71073 Å) at 296(2) K. The crystal structure was solved by direct methods and refined on F2 by full-matrix least-squares using Bruker's SHELXTL-97 [47]. The details of the crystallographic data for the synthesized compound are summarized in Table 1. Crystallographic data for the structural analysis have been deposited to the Cambridge Crystallographic Data Center under the number CCDC 2040959 for compound 1 and CCDC 2041071 for compound 2.

Hirshfeld surface analysis

Hirshfeld fingerprint plots were obtained from the program CrystalExplorer 17.5 [48]. Hirshfeld surface and contact enrichment ratios [49] were obtained with MoProViewer [50]. As X…Y and Y…X contacts yielded similar contact surfaces and Eelec values in the context of this study, the reciprocal contacts were merged together.

Table 1 Crystallographic data and details of refinement for compounds **1** and **2**

	Compound **1**	Compound **2**
Chemical formula	$C_{13}H_{13}BrN_2O_4$	$C_{13}H_{13}N_3O_6$
Formula weight (M)	341.16	325.28
Crystal system	Monoclinic	Orthorhombic
Space group	P121/n 1	Pna21
a (Å)	9.331(7)	16.88500
b (Å)	15.814(12)	7.14900
c (Å)	10.140(8)	24.42800
α (°)	90.00	90.00
β (°)	116.777(10)	90.00
γ ( )	90.00	90.00
V (Å^3)	1335.7(18)	2949
Z	4	8
Temperature (K)	298	298
Crystal size	0.257 × 0.202 × 0.199	0.105 × 0.089 × 0.067
Density (g/cm^3)	1.697	1.465
μ(Mo Kα)(mm^{-1})	3.093	0.121
F(000)	688	1360
Goodness of fit on F^2	1.044	0.984
R_1, $wR^{2\alpha}$ [$I > 2\sigma(I)$]	0.0331, 0.0810	0.0986, 0.2468
R_1, wR_2 (all data)	0.0402, 0.0846	0.1578, 0.2823
Residual electron density (max, min) e Å^{-3}	0.47	0.87
	−0.59	−0.44

$^{\alpha}R = \Sigma||F_o|-|F_c||/\Sigma|F_o|$; $wR(F^2) = [\Sigma w(|F_o|^2 - |F_c|^2)^2/\Sigma w|F_o|^4]^{1/2}$

Biological assay

The antifungal activity of synthesized dihydropyrimidine derivatives **1** and **2** was studied against *Candida albicans* and *Aspergillus niger* fungi by determining minimal inhibitory concentrations (MIC) by the twofold micro-dilution method as described in [51–57]. The compounds were prepared according to CLSI guidelines and diluted in U-bottom 96 well microtiter plates which contained Sabouraud liquid medium. The freshly prepared fungal strains at about 10^5 CFU (colony forming unit) in the above-mentioned medium were added to each well of the microplate and incubated at 37 °C for 24–48 h. The concentration of the tested compounds ranged from 1024 to 16 µg/mL. DMSO was used as a solvent. Fluconazole was used as a positive control, whereas DMSO was a negative control.

Computational approach

Computational calculations of the mentioned compounds were performed by using GaussView 6.0.16 [K1], Gaussian 16 ES64L-G16RevA.03 package program [K2]. The calculation level was selected as M062X/6-31G(d) level in the water. Conductor like the polarizable continuum (C-PCM) model was used to take into consideration of solute–solvent interactions. In the optimization calculations, no imaginary frequency was observed. The active sites of both compounds were determined using molecular electrostatic potential (MEP) maps.

Molecular docking

Molecular docking calculations were performed using Maestro 12.8 program. The related compounds were minimized using the LigPrep module. The target protein was selected as 5UIV from the protein data bank. This protein was prepared using Protein Preparation and Grid Generation modules. Then, docking calculation was performed using the Lig-Docking module. All calculations were done at the OPLS4 method at pH = 7 ± 2.

Results and discussion

Chemical synthesis

Synthesis of dihydropyrimidines was performed in the presence of low toxic cheaper triflate surrogate, viz., copper triflate (Fig. 1) [45]. The structures of synthesized dihydropyrimidines were determined by ^{1}H, ^{13}C NMR, mass spectroscopy (Figures 1S–6S), X-ray single-crystal diffraction method and elemental analysis. As it can be seen from ^{1}H NMR spectra, the signals from methyl and methoxy groups are observed at 2.27 and 3.49 ppm in the case of compound 1 and 2.3 and 3.49 ppm in the case of compound 2. The position of the dihydropyrimidine core CH group is at 5.39 and 5.48 ppm correspondingly. Their positions on ^{13}C NMR spectra are at 17.76, 48.78 and 50.7 ppm in the case of compound 1 and 17.80, 49.38 and 50.78 ppm in the case of compound 2. The signals from amine groups of dihydropyrimidine core are observed at 9.2 and 10.01 ppm in the case of compound 1 and 9.28 and 11.36 ppm in the case of compound 2.

Structure description

It was also possible to obtain single crystals of compounds **1** and **2**. Crystallographic data and detailed refinement results of the investigated compounds are presented in Table 1.

Molecular structure of methyl 4-(5-bromo-2-hydroxyphenyl)-6-methyl-2-oxo-1,2,3,4-tetrahydropyrimidine-5-carboxylate (1)

The compound **(1)** crystallizes in the monoclinic system with space group $P2_1/n$ and $Z = 4$. The molecule consists of a 1,2,3,4-tetrahydropyrimidine ring linked to a carboxylate group (COOMe), a methyl group and a 5-bromo-2-hydroxyphenyl ring (Fig. 2). Crystallographic data and detailed refinement results of the compound **(1)** appear in Table 1. The pertinent bond lengths and angles are listed in Table S1, while hydrogen bonds present in this structure are shown in Table S2. The crystal packing is shown in Fig. 9.

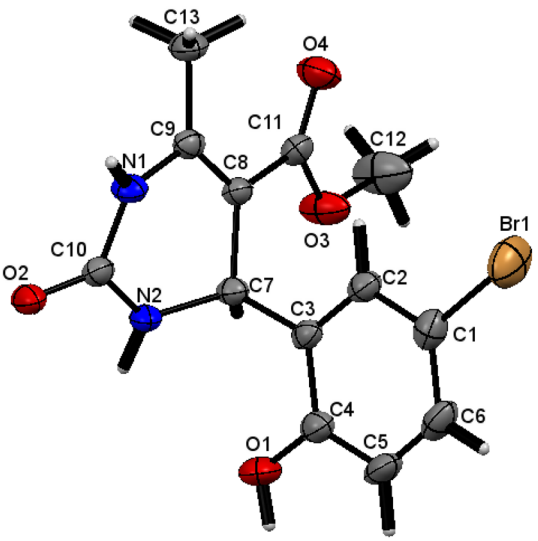

Fig. 2 View of the asymmetric unit of methyl 4-(5-bromo-2-hydroxyphenyl)-6-methyl-2-oxo-1,2,3,4-tetrahydropyrimidine-5-carboxylate (**1**), showing the atom labelling. Displacement ellipsoids are drawn at the 50% probability level

In the molecular structure of compound (**1**), molecules are linked via N–H···O [N1–H1A···O2^{ii} (−x+2, −y+1, −z+1)] hydrogen bonds forming inversion dimers with an $R_2^2(8)$ ring motif which involved the carbonyl group (C=O). Other inversion dimers are also linked via N–H···O=C (N2–H2···O1/O4^{i} ((i) x+½, −y+$^{3}/_{2}$, z+½) bifurcated hydrogen bonds and O–H…O=C [O1–H1···O2^{iii} ((iii) −x+2, −y+1, −z+2)] hydrogen bonds enclosing an $R_4^4(12)$ ring motif, involving the hydroxyl and the carbonyl groups, forming layers parallel to the (**b**,**c**) plane (Figs. 3, 4). Furthermore, weak N–H…Br interactions (involving H1A & H1A…Br1 = 3.416 Å), C-H…Br (involving H12C & H12A, the distances H12C…Br1 = 3.088 Å and H12A…Br1 = 3.804 Å) provide further stability to the crystal packing with C=O…Br (O…Br = 3.624 Å) (Fig. 5).

The aromatic moieties provide additional stability by the formation of C–H…π intramolecular interaction. The distances between the hydrogen atoms H12A, H12B and H12C and Cg (1 − *x*,1 − *y*,1 − *z*) which is the centroid of the C1–C2–C3–C4–C5–C6 aromatic ring are equal to 3.247, 2.883 and 3.740 Å (Fig. 5).

It is noteworthy that the phenyl rings C1–C2–C3–C4–C5–C6 in (**1**) exhibit a regular spatial configuration with normal C–C distances and C–C–C angles

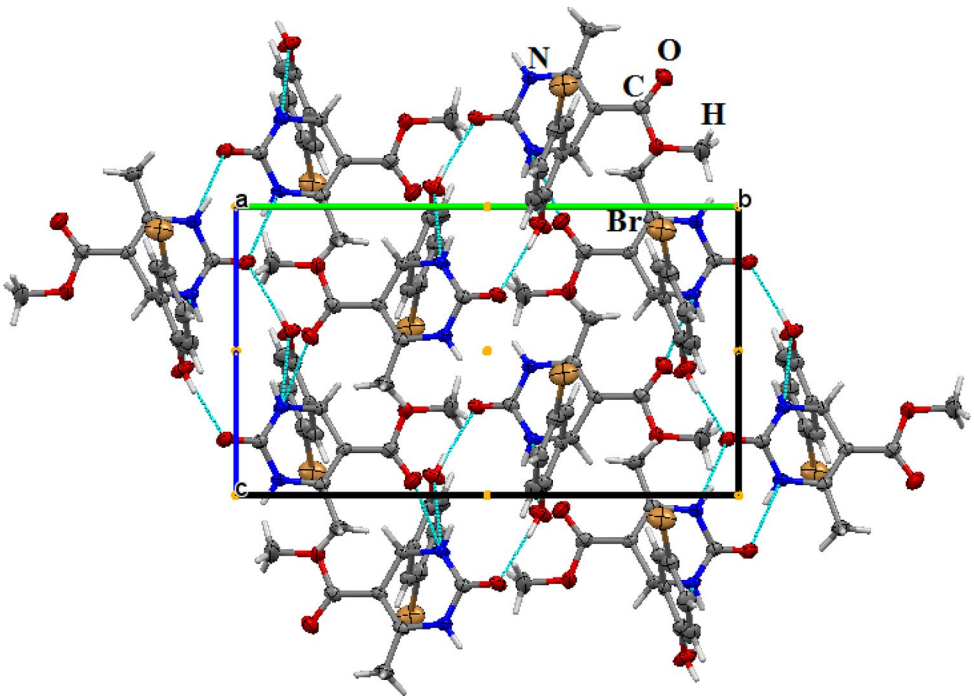

Fig. 3 A view along the *a*-axis of the crystal packing of the compound (**1**). The hydrogen bonds are shown as dashed lines. The inversion symmetry centres between molecules are shown by yellow points

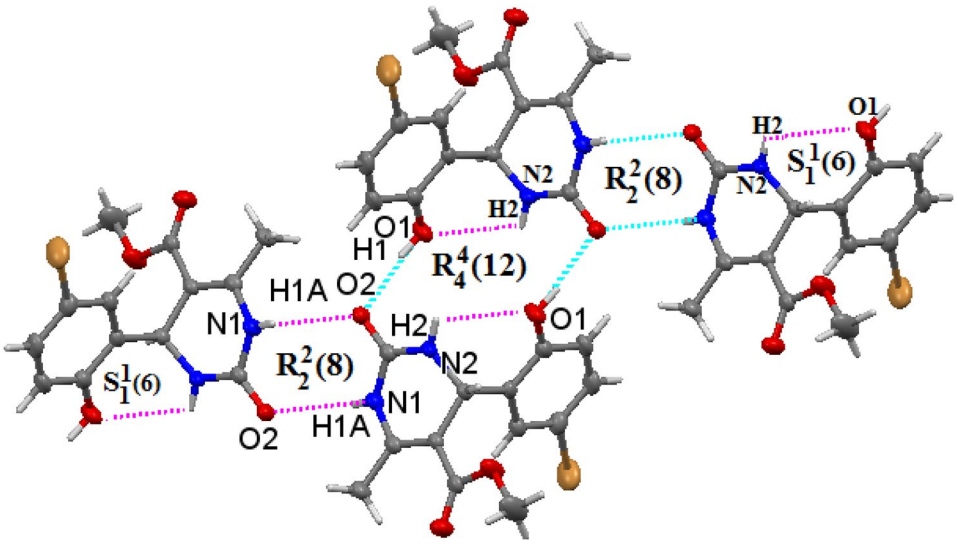

Fig. 4 Crystal structure of title compound (**1**) showing the dimers formed by N–H…O and O–H…O hydrogen bonds enclosing an $R_2^2(8)$, $R_4^4(12)$ and $S_1^1(6)$ ring motifs

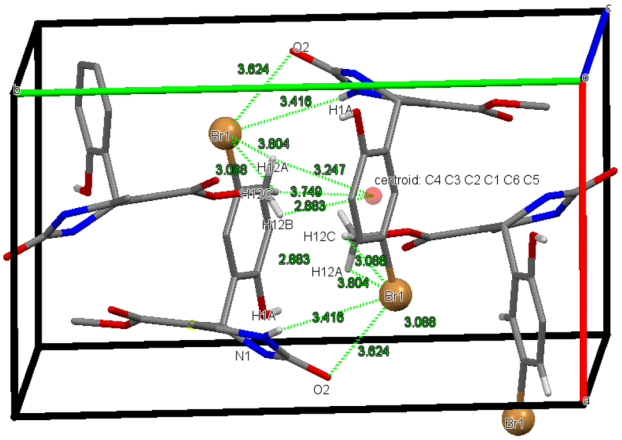

Fig. 5 Crystallographic packing diagram of compound **(1)** depicting N–H…Br, C–H…π and C=O…Br intermolecular interactions. The non-participating hydrogen atoms have been omitted for clarity

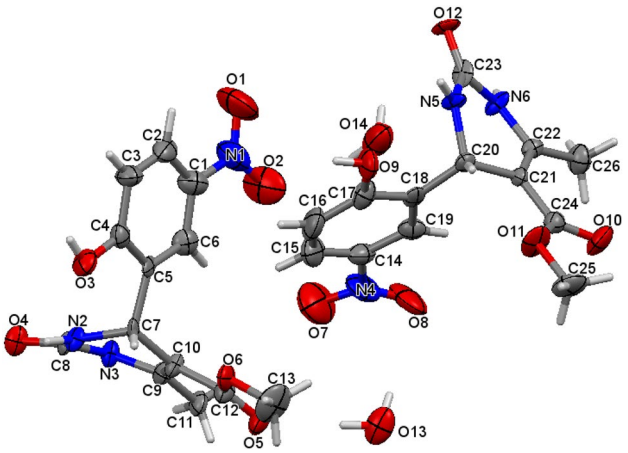

Fig. 6 A view of the asymmetric unit of methyl 4-(2-hydroxy-5-nitrophenyl)-6-methyl-2-oxo-1,2,3,4-tetrahydropyrimidine-5-carboxylate monohydrate, compound (**2**), showing the atom labelling. Displacement ellipsoids are drawn at the 50% probability level

(Table S1). The C–C bond lengths vary from 1.379 (4) to 1.406 (4) Å which are between a single and double bond and agree with those found for other similar compounds [58] and the C–C–C angles do not show any unusual values. For tetrahydropyrimidine, the C–N and C–C bond lengths are in the range of 1.331(3) to 1.513(3) Å. These values clearly agree well with those reported in other similar compounds [59]. The aryl substituents at the saturated carbon atom C7 have a pseudoaxial orientation with the C9–C8–C7–C3 torsion angle equal to − 96.4 (3)° and the C9–C8–C11–O3 torsion angle of − 168.4 (2)°.

It is of interest to note that the conformation of the tetrahydropyrimidine six-membered ring C7–C8–C9–N1–C10–N2 can be described in terms of Cremer and Pople puckering coordinates [60], i.e. evaluating the parameters Q (total puckering amplitude), $q2$, $q3$, θ and φ. The calculated values are as follows: $Q = 0.3173$ Å, $q2 = 0.3112$ Å, $q3 = -0.0617$ Å, $\theta = 101.22°$ and $\varphi = 178.58°$ for compound **(1)** which showed that the tetrahydropyrimidine ring has a half-chair conformation (C2) [61]. The conformation is stabilized by an intramolecular N–H…O–H hydrogen bond involving the N–H group adjacent to the aromatic ring with the hydroxyl substituent on the benzene ring (involving O1) forming an $S_1^1(6)$ motif.

Furthermore, the plane through the four coplanar atoms (N1, C10, C8 and C7) makes a dihedral angle of 77.54° with the phenyl ring. The carbonyl, carboxylate and methyl groups, except for the H atoms, are nearly coplanar with the attached heterocyclic ring [43, 58] and the bromine atom in this structure had equatorial orientation in the phenyl ring plane with torsion angles C3–C2–C1–Br1 and C5–C6–C1–Br1 equal to 179.11(19) and − 178.5°(2), respectively.

Molecular structure of methyl 4-(2-hydroxy-5-nitrophenyl)-6-methyl-2-oxo-1,2,3,4-tetrahydropyrimidine-5-carboxylate monohydrate (2)

The substitution of the bromo atom by the nitro group and the presence of water molecules introduce changes in the molecular conformation and crystal packing (Fig. 6). The compound **(2)** crystallizes in the orthorhombic system with space group $Pna2_1$ and $Z = 8$ (Table 1). Contrarily to compound **(1)**, the unit cell contains two geometrically independent molecules and two water molecules. The crystal packing is shown in Fig. 10.

Molecular conformation of tetrahydropyrimidine changes to the twisted boat for both molecules in compound **(2)** form describes in terms of Cremer and Pople puckering coordinates [60], i.e. evaluating the parameters Q, $q2$, $q3$, θ and φ. The calculated values of first molecule C7–N2–C8–N3–C9–C10 are as follows: $Q = 0.3727$ Å, $q_2 = 0.3576$ Å, $q_3 = 0.1049$ Å, $\theta = 73.66°$ and $\varphi = 6.51°$ and for second molecule C20–C21–C22–N6–C23–N5, the calculated values are $Q = 0.3736$ Å, $q_2 = 0.3625$ Å, $q_3 = 0.0905$ Å, $\theta = 75.98°$ and $\varphi = -7.24°$.

The bond lengths and bond angles in this molecular structure, listed in Table S3, are also close to standard values, similar to the previous structure of compound **(1)** and comparable to related structures of literature [62, 63].

In the structural arrangement, hydrogen bonds play an important role in stabilizing the structure. Thus, the presence of water molecules in the crystal packing interferes with the interaction of the carboxylate and nitro groups giving rise to a rich network of hydrogen bonds (Table S4). The molecules are interconnected via N–H…O and O–H…O hydrogen bonds generated by the H_2O13 and H_2O14 crystallization water molecules to form layers spreading along [010] direction (Fig. 7).

The crystallization water molecules are connected to nitro groups (O13–H13E···O8 and O14–H14A···O2) and to the carboxylate group of each tetrahydropyrimidine. The molecules are connected through hydroxyl groups to water molecules involving O9 and O3 (O9–H9···O14^{i} ((i) x, $y-1$, z) & O3–H3···O13^{ii} ((ii) $x+½, -y+½, z$)

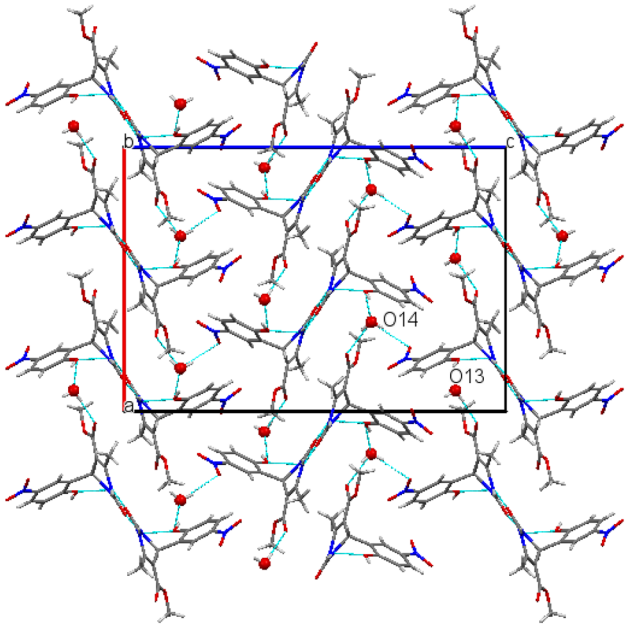

Fig. 7 A view along the **b** axis of the crystal packing of compound **(2)**. The hydrogen bonds are shown as dashed lines

(Table S4). The aromatic moieties provide additional stability by the formation of C–H…π intramolecular interaction. The distances between the hydrogen atoms and centroids are 3.321 and 3.955 Å (Fig. 8). Intermolecular stacking interactions between aromatic rings are absent in both compounds **(1)** & **(2)**.

Hirshfeld surface analysis

The fingerprint plots of the intermolecular interactions for both compounds (**1**) and (**2**) show two spikes at short distances due to the H..O and O…H reciprocal hydrogen bonds (Figures 7S and 8S). This is the case for the two independent molecules (**2**a) and (**2**b) present in the asymmetric unit of compound (**2**) crystal.

For compound (**1**), the main interactions are H…H contacts and weak hydrogen bonds Br…H as well as H…π (H…C and H…N). The three strong H-bond donors (2 H–N and 1 H–O) form three strong H-bonds with the three strong oxygen acceptors (a hydroxyl and two carbonyl groups). The aromatic rings are essentially interacting with the methyl and > CH aromatic hydrogen atoms.

The contact enrichment (Tables 2, 3), derived from the Hirshfeld surface, is computed from the ratio of the actual contacts C_{xy} in the crystal with those computed as if all types of contacts had the same probability to form [50]. An enrichment ratio larger than unity for a given pair of chemical species X … Y indicates that these contacts are favoured (over-represented) in the crystal. In compound (**1**), the O…Ho/n contact is the most enriched and corresponds to the two N–H…O and the O–H…O strong hydrogen bonds. The Hc…C contacts are the most abundant in Table 2 and are a little enriched at $E = 1.31$. The bromine atom is essentially in contact with aromatic rings resulting in significantly enriched C…Br contacts and, at a long distance, with some Hc atoms (Fig. 9).

For compound (**2**), the major contacts are C…Hc and O…Hc (more than 19% of the surface) followed by O…Hn/o and

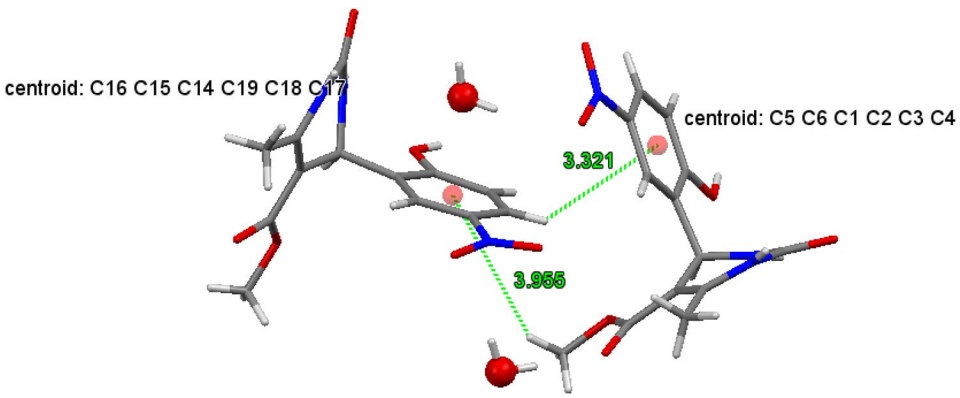

Fig. 8 C-H…π intermolecular interactions in the structure of compound **(2)**

Table 2 Surface content and nature of contacts on the Hirshfeld surface of compound (1)

Atom	Ho/n	C	N	O	Br	Hc
Atom…ALL %	11.0	22.8	2.0	14.2	13.9	36.1
ALL…Atom %	11.1	21.0	1.7	14.1	14.8	37.3
Ho/n	1.0				% contacts	
C	1.8	2.9			*C*xy	
N	0.2	0.1	0.0			
O	**9.8**	3.2	0.6	0.2		
Br	3.1	**11.8**	1.0	3.6	0.0	
Hc	5.3	**21.1**	1.9	**10.8**	9.1	12.7
Ho/n	0.8				Enrichment	
C	0.37	0.61			*E*xy	
N	0.38	0.11	-			
O	**3.12**	0.51	1.13	0.09		
Br	0.99	**1.88**	1.89	0.89	0	
Hc	0.65	**1.31**	1.37	1.04	0.87	0.94

Reciprocal contacts *X*–*Y* and *Y*–*X* were merged. The major contacts C_{XY} and the major enriched ones (E_{XY} larger than unity) are in bold characters. Hydrogen atoms bound to nitrogen or oxygen are distinguished from the more hydrophobic Hc atoms bound to carbon

Table 3 Contact proportions C_{xy} and their enrichments E_{xy} for compound (**2**)

Atom	Ho/n	C	N	O	Hc
Atom…ALL %	10.1	24.5	3.4	27.2	34.9
ALL…Atom %	18.7	20.5	2.6	27.9	30.3
Ho/n	1.3				
C	1.5	6.4			
N	0.9	0.3	0.0		
O	**16.7**	**10.7**	1.5	3.6	
Hc	7.1	**19.8**	3.3	**19.0**	7.9
Ho/n	0.69				
C	0.22	1.26			
N	0.97	0.26	0		
O	**2.12**	0.86	0.88	0.48	
Hc	0.74	**1.36**	1.72	1.06	0.75

Hirshfeld's surface was generated around an ensemble of two independent molecules, not in contact with each other in the crystal packing. The major contacts C_{XY} and the major enriched ones (E_{XY} larger than unity) are in bold characters

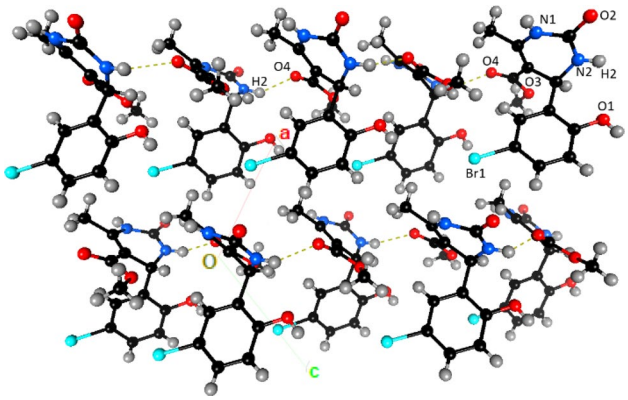

Fig. 9 Crystallographic autostereogram of crystal packing for compound (**1**) along **b** axis. Horizontal translations correspond to **a** + **c**

O…C (Table 3). The less hydrophilic oxygen atoms of the nitro group interact mostly with Hc and C atoms (Fig. 10). The major enriched contacts are the strong H-bonds O…Hn/o and the weak H-bonds C…Hc.

When the Hirshfeld surface of the two independent molecules is compared (data not shown), they show similar contact types, with the two proportions C_{xy} sets 98.6% correlated and the two E_{xy} sets 88.7% correlated.

It is important to specify how atoms located inside the Hirshfeld surface (HS) interact with the atoms of molecules located in the neighbouring as it provides information about the packing contacts of molecules [64–68]. For compound **I**, the reciprocal Atom…ALL and ALL…Atom surfaces are similar, as the Hirshfeld surface was computed on the molecule constituting the asymmetric unit (Table 1). Here, ALL stands for all the atoms of molecules located in the surrounding of the HS. It is found that the H atoms located inside the HS interact the most with the atoms of molecules located outside HS as compared to other atoms present inside the HS. The contribution of H-ALL interactions is found to be close to one half in proportion, but the percentage of hydrophilic Ho/n atom is only 11% on the surface. The other interactions are C-ALL (22.8%), O-ALL (14.2%), Br-ALL (13.9.4%) and N-ALL (2.0%).

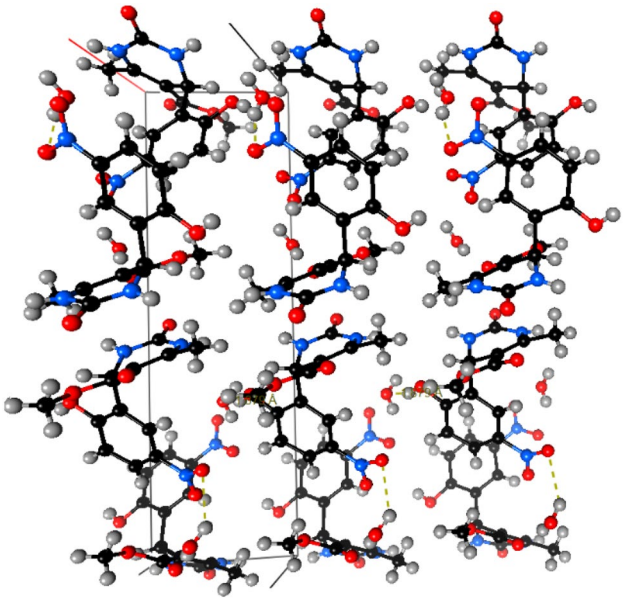

Fig. 10 Crystallographic autostereogram of crystal packing for compound (**2**), **b** is horizontal and **c** is vertical

For compound **II**, the reciprocal Atom…ALL and ALL…Atom surfaces are more dissimilar, as the Hirshfeld surface was computed around the two independent organic molecules present in the asymmetric unit, while the HS around the two water molecules was not computed (Table 2). The H…ALL contacts represent also the major interaction, reaching 45% in percentage, with again only 10% of the HS related to the hydrophilic Hn/o atoms. The proportions of the other contacts are O-ALL (27.2%), C-ALL (14.2%) and N-ALL (3.4%). The proportion of Ho/n…ALL contacts at 18.7% are much larger than the reciprocal contact surface ALL…Ho/n as the water molecules providing the H–O hydrogen atoms are not contributing to the inner side of the Hirshfeld surface.

The response of a crystal to applied stress or force depends on the voids in the crystal packing. When voids are small, the atoms are strongly packed with each other and the crystal can bear the stress of a significant amount. The voids were computed by using CrystalExplorer software (Fig. 11). For compound **I**, the void volume and surface area were found to be 123.9 $Å^3$ and 472.3 $Å^2$, respectively. The voids occupy only 9.2% in the percentage of the space in the crystal packing which is an indication that the molecules are strongly held with each other through non-covalent interactions [69–73].

For compound **II**, the void volume and surface area are, respectively, 351.6 $Å^3$ and 1082 $Å^2$, which results in a slightly higher 11.9% proportion of void in the unit cell, compared to compound **I**, but corresponds to a still tightly packed crystal.

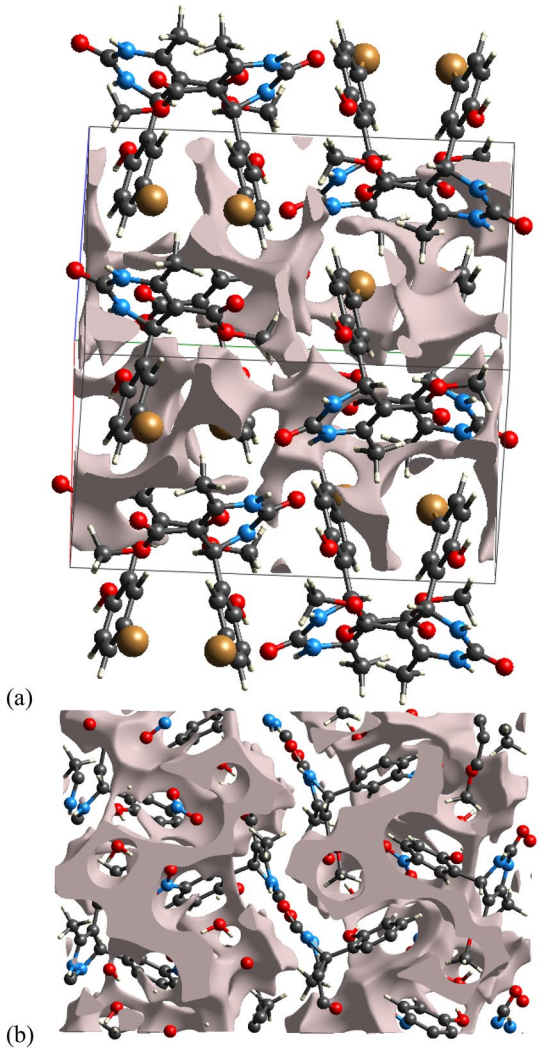

Fig. 11 Void surface in the crystal packing at 0.002 a.u. electron density. **a** Of compound **I** (**b** horizontal), **b** of compound **II** (**c** horizontal, **a** vertical)

Biological assays

The antifungal activity of synthesized dihydropyrimidine derivatives **1** and **2** was studied against *Candida albicans* and *Aspergillus niger* fungi. The twofold micro-dilution method was used to determine the minimum inhibitory

Table 4 Minimum inhibitory concentration (MIC, μg/μL) of the studied compounds

Bacteria	Minimum inhibitory concentration (MIC, μg/μL)		
	Compound (**1**)	Compound (**2**)	Fluconazole
Candida albicans	32	64	32
Aspergillus niger	32	16	32

concentration (MIC) of the synthesized compounds **1** and **2** as well as a pristine antibiotic (fluconazole). As shown in Table 4, the synthesized dihydropyrimidine **1** demonstrated similar to fluconazole activity in the case of *Candida albicans* and *Aspergillus niger* (32 µg/µL) fungi. MIC of compound (**2**) was lower than fluconazole result (64 µg/µL) in the case of *Candida albicans,* whereas in the case of *Aspergillus niger* it was 2 times higher (16 µg/µL).

Due to the fact that the solvent (DMSO) is an example of a substance that can display biological activity, the results were also recorded using pure DMSO that did not contain the investigated molecules. It was discovered that DMSO has no effect on the fungi indicated above.

Computational analyses

Studied compounds are optimized M062X/6-31G(d) level. No imaginary frequency is observed at the end of the calculations. Optimized structures of the mentioned compounds are represented in Fig. 12.

According to Fig. 12, the structures are not planar and the direction of functional groups is similar to each other in both compounds. The IR spectrum of them is calculated and represented in Fig. 13.

According to Fig. 13, there are no big differences. The obtained frequencies are 3643, 3504, 1833, 1748, 1530, 1405, 1296, 1167 and 590 cm^{-1} for compound **1**; 3644, 3418, 1836, 1718, 1446, 1291, 1166 and 597 cm^{-1} for compound **2**. According to Fig. 13, the structures are at the ground state due to the no imaginary frequency. Additionally, MEP maps of both compounds are calculated to determine the active region on the molecular surface. They are represented in Fig. 14.

According to the MEP map (Fig. 14), compound **2** is seen as more active than the other one. The environment of heteroatoms especially oxygen atoms is mainly red and yellow. It means that these regions can interact easily. On the other hand, the environment of hydrogen atoms is mainly dark blue.

Molecular docking

It is very significant to obtain pre-information about the biological activity of chemicals. For this purpose, there are several analyses are used among which quantum chemical descriptors, quantitative structure–activity relationship, Fukui functions, etc., can be mentioned. But the best one is molecular docking [74, 75]. However, the target protein and its receptor-binding domain (RBD) should be known. The thymidylate kinase of *Candida albicans* was selected as a target protein in this study. The target protein (PDB ID: 5UIV) and its RBD are represented in Fig. 15, whereas the docking score (DS), van der Waals energy (E_{vdW}), coulomb energy (E_{Coul}) and total interaction energy (E_{Total}) are given in Table 5.

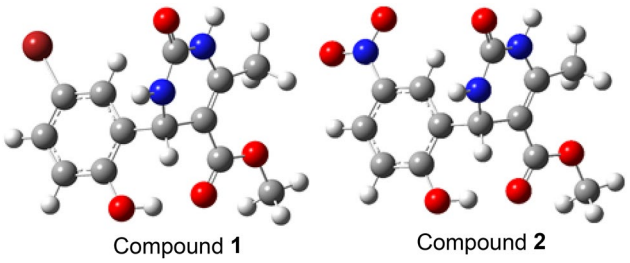

Fig. 12 The optimized structures of studied compounds

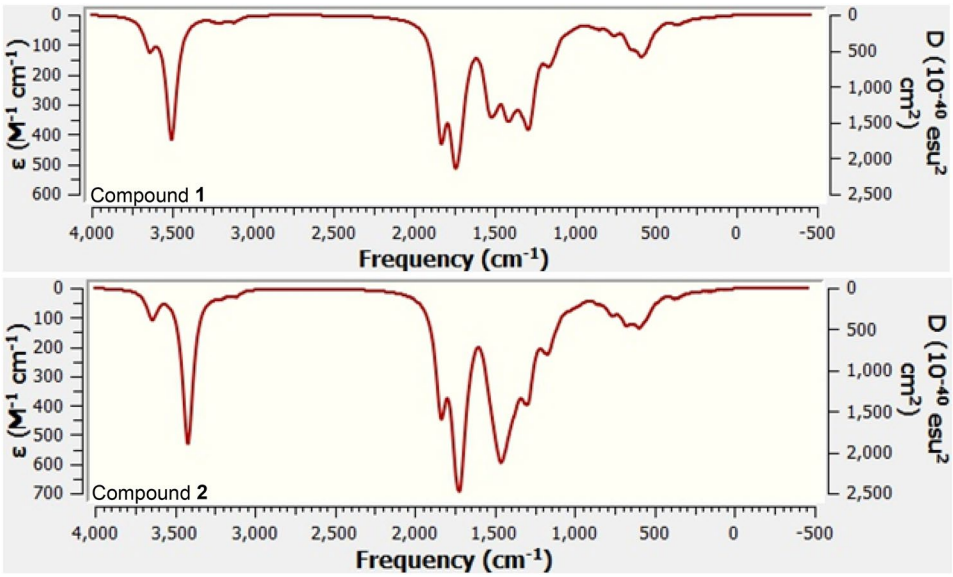

Fig. 13 The calculated IR spectrum of compounds **1** and **2**

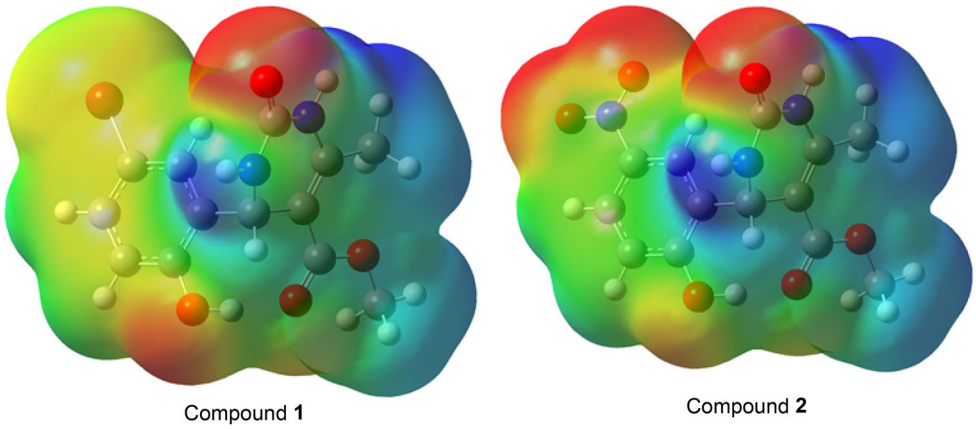

Fig. 14 MEP map of compounds **1** and **2**

Fig. 15 Structure of 5UIV and its RBD

Table 5 The molecular docking result

Compound	DS[a]	E_{vdW}[a]	E_{Coul}[a]	E_{Total}[a]
1	−5.08	−27.34	−3.67	−31.01
2	−4.79	−22.07	−5.86	−27.92

[a]In kcal/mol

According to Table 5, the key-lock compatibility in compound **1** is better than in compound **2** due to the docking score. Additionally, total interaction energy and chemical interactions are better in compound **1**, too. As a result, it can be said that the antifungal activity of compound **1** against *Candida albicans* is better than that of compound **2**. This result is in agreement with experimental results (Table 4).

According to the represented docking and interaction structures (Fig. 16), dominant interaction types are as follows: H-bond, pi–pi stacking, pi-cation, negative and positive charged, polar and metal interactions. The studied compounds interact with the magnesium at the RBD of 5UIV.

Conclusion

The salicylaldehyde-based dihydropyrimidine derivatives **1** and **2** were synthesized by Biginelli reaction in microwave conditions in the presence of low toxic cheaper copper triflate surrogate. The structure of synthesized dihydropyrimidines was investigated by X-ray single-crystal diffraction and the presence of non-covalent interactions and their impact on crystal packing and conformation of dihydropyrimidine ring were revealed. Along with it, Hirshfeld surface analysis was carried out to gain insight into crystal packing and molecular interactions. Considering that the proposed substances **1** and **2** can have the ability to act as an antifungal drug, it was tested for the biological activity against *Candida albicans* and *Aspergillus niger*, as well as, was made a comparison with the activity of pristine antibiotic fluconazole. According to the antifungal activity results, compounds **1** and **2** demonstrate pronounced antifungal activity, which is also in agreement with the performed computational calculations. As a result of the obtained data, it is possible to conclude that in future, applying innovative technologies can lead to the creation and development of new effective antifungal drugs on the basis of these compounds.

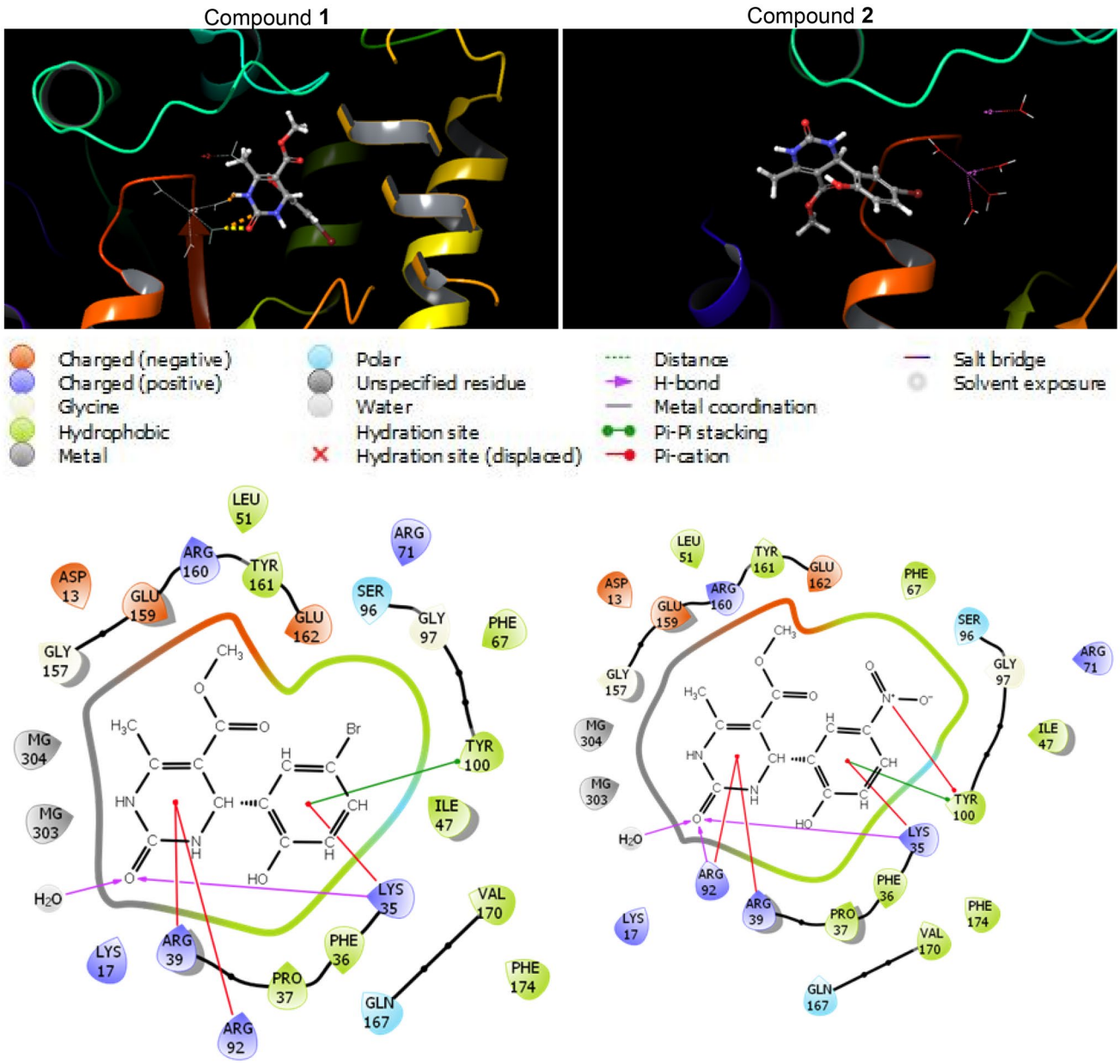

Fig. 16 Docking and interaction structures of studied compounds

Supplementary Information The online version contains supplementary material available at https://doi.org/10.1007/s13738-022-02659-9.

Acknowledgements This study was made possible by TUBITAK ULAKBIM, High Performance and Grid Computing Center (TR-Grid e-Infrastructure).

Funding This work was supported by the Erasmus + overseas/ICM KA107 programme, Science Development Foundation under the President of the Republic of Azerbaijan and TUBITAK in the frames of the project number EIF-BGM-5-AZTURK-1/2018-2/02/4-M-02 and the Scientific Research Project Fund of Sivas Cumhuriyet University under Project Number RGD-020.

Declarations

Conflict of interest The authors declare that they have no known competing financial interests or personal relationships that could have appeared to influence the work reported in this paper.

References

1. P. Biginelli, The urea-aldehyde derivatives of acetoacetic esters. Gazz. Chim. Ital **23**, 360–416 (1893)

2. C.O. Kappe, Recent advances in the Biginelli dihydropyrimidine synthesis. New tricks from an old dog. Acc Chem Res **33**(12), 879–888 (2000). https://doi.org/10.1021/ar000048h
3. Li S, et al. Dihydropyrimidine compounds and their uses in preparation of medicaments for treating and preventing antiviral diseases. U.S. Patent No. 8,168,642. 2012.
4. T. Watabe, K. Ogura, T. Nishiyama, Molecular toxicological mechanism of the lethal interactions of the new antiviral drug, sorivudine, with 5-fluorouracil prodrugs and genetic deficiency of dihydropyrimidine dehydrogenase. Yakugaku zasshi J. Pharm. Soc. Jpn. **122**(8), 527 (2002). https://doi.org/10.1248/yakushi.122.527
5. F.M. Awadallah et al., Synthesis of some dihydropyrimidine-based compounds bearing pyrazoline moiety and evaluation of their antiproliferative activity. Eur. J. Med. Chem. **70**, 273–279 (2013). https://doi.org/10.1016/j.ejmech.2013.10.003
6. S. Oie et al., Alteration of dihydropyrimidine dehydrogenase expression by IFN-α affects the antiproliferative effects of 5-fluorouracil in human hepatocellular carcinoma cells. Mol. Cancer Ther. **6**(8), 2310–2318 (2007). https://doi.org/10.1158/1535-7163.MCT-06-0281
7. E. Klein et al., New chemical tools for investigating human mitotic kinesin Eg5. Bioorg. Med. Chem. **15**(19), 6474–6488 (2007). https://doi.org/10.1016/j.bmc.2007.06.016
8. H.Y.K. Kaan et al., Structural basis for inhibition of Eg5 by dihydropyrimidines: stereoselectivity of antimitotic inhibitors enastron, dimethylenastron and fluorastrol. J. Med. Chem. **53**(15), 5676–5683 (2010). https://doi.org/10.1021/jm100421n
9. C.M. Wright et al., Pyrimidinone-peptoid hybrid molecules with distinct effects on molecular chaperone function and cell proliferation. Bioorg. Med. Chem. **16**(6), 3291–3301 (2008). https://doi.org/10.1016/j.bmc.2007.12.014
10. O.C. Agbaje et al., Synthesis and in vitro cytotoxicity evaluation of some fluorinated hexahydropyrimidine derivatives. Bioorg. Med. Chem. Lett. **21**(3), 989–992 (2011). https://doi.org/10.1016/j.bmcl.2010.12.022
11. B.R.P. Kumar et al., Novel Biginelli dihydropyrimidines with potential anticancer activity: a parallel synthesis and CoMSIA study. Eur. J. Med. Chem. **44**(10), 4192–4198 (2009). https://doi.org/10.1016/j.ejmech.2009.05.014
12. D.A. Ibrahim, A.M. El-Metwally, Design, synthesis, and biological evaluation of novel pyrimidine derivatives as CDK2 inhibitors. Eur. J. Med. Chem. **45**(3), 1158–1166 (2010). https://doi.org/10.1016/j.ejmech.2009.12.026
13. A. Wang et al., New magnetic nanocomposites of ZrO_2–Al_2O_3–Fe_3O_4 as green solid acid catalysts in organic reactions. Catal. Sci. Technol. **4**(1), 71–80 (2014). https://doi.org/10.1039/C3CY00572K
14. B.K. Ghosh, S. Hazra, N.N. Ghosh, Synthesis of Cu@CF@SBA15: a versatile catalysts for (i) reduction of dyes, trifluralin, synthesis of (ii) DHPMs by Biginelli reaction and (iii) 1,2,3-triazole derivatives by 'Click reaction.' Catal. Commun. **80**, 44–48 (2016). https://doi.org/10.1016/j.catcom.2016.03.016
15. N. October et al., Reversed chloroquines based on the 3,4-dihydropyrimidin-2(1H)-one scaffold: synthesis and evaluation for antimalarial, β-haematin inhibition, and cytotoxic activity. ChemMedChem **3**(11), 1649–1653 (2008). https://doi.org/10.1002/cmdc.200800172
16. S. Fatima et al., One pot efficient diversity oriented synthesis of polyfunctional styryl thiazolopyrimidines and their bio-evaluation as antimalarial and anti-HIV agents. Eur. J. Med. Chem. **55**, 195–204 (2012). https://doi.org/10.1016/j.ejmech.2012.07.018
17. H. Kaur et al., Primaquine–pyrimidine hybrids: synthesis and dual-stage antiplasmodial activity. Eur. J. Med. Chem. **101**, 266–273 (2015). https://doi.org/10.1016/j.ejmech.2015.06.045
18. T.N. Akhaja, J.P. Raval, 1,3-Dihydro-2H-indol-2-ones derivatives: design, synthesis, in vitro antibacterial, antifungal and antitubercular study. Eur. J. Med. Chem. **46**(11), 5573–5579 (2011). https://doi.org/10.1016/j.ejmech.2011.09.023
19. R.K. Yadlapalli et al., Synthesis and in vitro anticancer and antitubercular activity of diarylpyrazole ligated dihydropyrimidines possessing lipophilic carbamoyl group. Bioorg. Med. Chem. Lett. **22**(8), 2708–2711 (2012). https://doi.org/10.1016/j.bmcl.2012.02.101
20. S.N. Mokale et al., Synthesis and anti-inflammatory activity of some 3-(4,6-disubtituted-2-thioxo-1,2,3,4-tetrahydropyrimidin-5-yl) propanoic acid derivatives. Bioorg. Med. Chem. Lett. **20**(15), 4424–4426 (2010). https://doi.org/10.1016/j.bmcl.2010.06.058
21. S.S. Bahekar, D.B. Shinde, Synthesis and anti-inflammatory activity of some [4,6-(4-substituted aryl)-2-thioxo-1,2,3,4-tetrahydro-pyrimidin-5-yl]-acetic acid derivatives. Bioorg. Med. Chem. Lett. **14**(7), 1733–1736 (2004). https://doi.org/10.1016/j.bmcl.2004.01.039
22. B.A. Marathwada, Synthesis and anti-inflammatory activity of some [2-amino-6-(4-substituted aryl)-4-(4-substituted phenyl)-1, 6-dihydropyrimidine-5-yl]-acetic acid derivatives. Acta Pharm **53**, 223–229 (2003)
23. A.R. Trivedi et al., Novel dihydropyrimidines as a potential new class of antitubercular agents. Bioorg. Med. Chem. Lett. **20**(20), 6100–6102 (2010). https://doi.org/10.1016/j.bmcl.2010.08.046
24. A.M. Maharramov et al., Synthesis, investigation of the new derivatives of dihydropyrimidines and determination of their biological activity. J. Mol. Struct. **1141**, 39–43 (2017). https://doi.org/10.1016/j.molstruc.2017.03.084
25. U. Rashid et al., Structure based medicinal chemistry-driven strategy to design substituted dihydropyrimidines as potential antileishmanial agents. Eur. J. Med. Chem. **115**, 230–244 (2016). https://doi.org/10.1016/j.ejmech.2016.03.022
26. K.S. Atwal et al., Dihydropyrimidine calcium channel blockers: 2-heterosubstituted 4-aryl-1, 4-dihydro-6-methyl-5-pyrimidinecarboxylic acid esters as potent mimics of dihydropyridines. J. Med. Chem. **33**(5), 1510–1515 (1990). https://doi.org/10.1021/jm00167a035
27. I.S. Zorkun et al., Synthesis of 4-aryl-3, 4-dihydropyrimidin-2 (1H)-thione derivatives as potential calcium channel blockers. Bioorg. Med. Chem. **14**(24), 8582–8589 (2006). https://doi.org/10.1016/j.bmc.2006.08.031
28. R.V. Chikhale et al., Synthesis and pharmacological investigation of 3-(substituted 1-phenylethanone)-4-(substituted phenyl)-1, 2, 3, 4-tetrahydropyrimidine-5-carboxylates. Eur. J. Med. Chem. **44**(9), 3645–3653 (2009). https://doi.org/10.1016/j.ejmech.2009.02.021
29. R.W. Lewis et al., Dihydropyrimidinone positive modulation of δ-subunit-containing γ-aminobutyric acid type A receptors, including an epilepsy-linked mutant variant. Biochemistry **49**(23), 4841–4851 (2010). https://doi.org/10.1021/bi100119t
30. L. Figueroa-Valverde et al., Activity induced by two steroid-dihydropyrimidine derivatives on glucose levels in a diabetic rat model. Relationship between descriptors logP and π and its antidiabetic activity. Int. J. PharmTech Res. **2**, 2075–2080 (2010)
31. A.D. Patel et al., Molecular docking, in-silico ADMET study and development of 1,6-dihydropyrimidine derivative as protein tyrosine phosphatase inhibitor: an approach to design and develop antidiabetic agents. Curr. Comput. Aided Drug Des. **14**(4), 349–362 (2018). https://doi.org/10.2174/1573409914666180426125721
32. A.D. Patil et al., Novel alkaloids from the sponge Batzella sp.: inhibitors of HIV gp120-human CD4 binding. J. Org. Chem. **60**(5), 1182–1188 (1995). https://doi.org/10.1021/jo00110a021
33. K.B. Mehtaa, R.K.P.H.S. Joshic, In silico study of novel dihydropyrimidines against anti cancer, anti tuberculosis, anti HIV and anti malarial activity. Int. J. Scient. Eng. Res **4**, 1–8 (2013)

34. S. Terracciano et al., Structural insights for the optimization of dihydropyrimidin-2 (1H)-one based mPGES-1 inhibitors. ACS Med. Chem. Lett. **6**(2), 187–191 (2015). https://doi.org/10.1021/ml500433j
35. B.K. Singh et al., Synthesis of 2-sulfanyl-6-methyl-1, 4-dihydropyrimidines as a new class of antifilarial agents. Eur. J. Med. Chem. **43**(12), 2717–2723 (2008). https://doi.org/10.1016/j.ejmech.2008.01.038
36. J.C. Barrow et al., In vitro and in vivo evaluation of dihydropyrimidinone C-5 amides as potent and selective α1A receptor antagonists for the treatment of benign prostatic hyperplasia. J. Med. Chem. **43**(14), 2703–2718 (2000). https://doi.org/10.1021/jm990612y
37. X. Zhu et al., 2,4-Diaryl-4,6,7,8-tetrahydroquinazolin-5 (1H)-one derivatives as anti-HBV agents targeting at capsid assembly. Bioorg. Med. Chem. Lett. **20**(1), 299–301 (2010). https://doi.org/10.1016/j.bmcl.2009.10.119
38. G.C. Rovnyak, K.S. Atwal, A. Hedberg, S.D. Kimball, S. Moreland, J.Z. Gougoutas, B.C. O'Reilly, J. Schwartz, M.F. Malley, Dihydropyrimidine calcium channel blockers. 4. Basic 3-substituted-4-aryl-1,4-dihydropyrimidine-5-carboxylic acid esters. Potent antihypertensive agents. J. Med. Chem. **35**(17), 3254–3263 (1992). https://doi.org/10.1021/jm00095a023
39. H.J. Finlay et al., Discovery of ((S)-5-(Methoxymethyl)-7-(1-methyl-1 H-indol-2-yl)-2-(trifluoromethyl)-4, 7-dihydropyrazolo [1, 5-a] pyrimidin-6-yl)((S)-2-(3-methylisoxazol-5-yl) pyrrolidin-1-yl) methanone As a Potent and Selective IKur Inhibitor. J. Med. Chem. **55**(7), 3036–3048 (2012). https://doi.org/10.1021/jm201386u
40. J. Lloyd et al., Pyrrolidine amides of pyrazolodihydropyrimidines as potent and selective KV1.5 blockers. Bioorg Med Chem Lett **20**(4), 1436–1439 (2010). https://doi.org/10.1016/j.bmcl.2009.12.085
41. J. Lloyd et al., Dihydropyrazolopyrimidines containing benzimidazoles as KV1.5 potassium channel antagonists. Bioorg Med Chem Lett **19**(18), 5469–5473 (2009). https://doi.org/10.1016/j.bmcl.2009.07.083
42. W.C. Wong et al., Design and synthesis of novel α1a adrenoceptor-selective antagonists. 4. Structure—activity relationship in the dihydropyrimidine series. J Med Chem **42**(23), 4804–4813 (1999). https://doi.org/10.1021/jm9902032
43. A.E. Huseynzada et al., Synthesis, crystal structure and antibacterial properties of 6-methyl-2-oxo-4-(quinolin-2-yl)-1,2,3,4-tetrahydropyrimidine-5-carboxylate. J. Mol. Struct. **1219**, 128581 (2020). https://doi.org/10.1016/j.molstruc.2020.128581
44. A.E. Huseynzada et al., Synthesis, crystal structure and antibacterial studies of 2,4,6-trimetoxybenzaldehyde based dihydropyrimidine derivatives. J. Mol. Struct. (2021). https://doi.org/10.1016/j.molstruc.2021.130678
45. A.E. Huseynzada et al., Synthesis, crystal structure and antibacterial studies of dihydropyrimidines and their regioselectively oxidized products. RSC Adv. **11**(11), 6312–6329 (2021). https://doi.org/10.1039/D0RA10255E
46. K. Dutta et al., Synergistic interplay of covalent and non-covalent interactions in reactive polymer nanoassembly facilitates intracellular delivery of antibodies. Angew. Chem. Int. Ed. **60**(4), 1821–1830 (2021). https://doi.org/10.1002/anie.202010412
47. G.M. Sheldrick, *SHELXTL V5.1, Software reference manual* (Bruker AXS Inc, Madison, 1997), pp.1–250
48. C.F. Mackenzie et al., CrystalExplorer model energies and energy frameworks: extension to metal coordination compounds, organic salts, solvates and open-shell systems. IUCrJ **4**(5), 575–587 (2017). https://doi.org/10.1107/S205225251700848X
49. B. Guillot, E. Enrique, L. Huder, C. Jelsch, MoProViewer: a tool to study proteins from a charge density science perspective. Acta Cryst. **A70**, C279 (2014)
50. C. Jelsch, K. Ejsmont, L. Huder, The enrichment ratio of atomic contacts in crystals, an indicator derived from the Hirshfeld surface analysis. IUCrJ **1**(2), 119–128 (2014). https://doi.org/10.1107/S2052252514003327
51. J.G. Vincent, H.W. Vincent, J. Morton, Filter paper disc modification of the oxford cup penicillin determination. Proc. Soc. Exp. Biol. Med. **55**(3), 162–164 (1944). https://doi.org/10.3181/00379727-55-14502
52. A.A. Ardakani et al., Synthesis, characterization, crystal structures and antibacterial activities of some Schiff bases with N_2O_2 donor sets. J. Iran. Chem. Soc. **15**(7), 1495–1504 (2018). https://doi.org/10.1016/j.ica.2021.120677
53. H. Kargar et al., Nickel (II), copper (II) and zinc (II) complexes containing symmetrical Tetradentate Schiff base ligand derived from 3, 5-diiodosalicylaldehyde: synthesis, characterization, crystal structure and antimicrobial activity. J. Iran. Chem. Soc. **18**(9), 2493–2503 (2021). https://doi.org/10.1080/00958972.2021.1900831
54. A. Sahraei et al., Synthesis, characterization, crystal structures and biological activities of eight-coordinate zirconium (IV) Schiff base complexes. Transition Met. Chem. **42**(6), 483–489 (2017). https://doi.org/10.1016/j.molstruc.2017.08.022
55. A. Sahraei et al., Distorted square-antiprism geometry of new zirconium (IV) Schiff base complexes: synthesis, spectral characterization, crystal structure and investigation of biological properties. J. Mol. Struct. **1149**, 576–584 (2017). https://doi.org/10.1007/s11243-017-0152-x
56. H. Kargar et al., Some new Cu(II) complexes containing O, N-donor Schiff base ligands derived from 4-aminoantipyrine: synthesis, characterization, crystal structure and substitution effect on antimicrobial activity. J. Coord. Chem. **74**(9–10), 1534–1549 (2021). https://doi.org/10.1007/s13738-021-02207-x
57. H. Kargar et al., Binuclear Zn(II) Schiff base complexes: synthesis, spectral characterization, theoretical studies and antimicrobial investigations. Inorg. Chim. Acta **530**, 120677 (2022). https://doi.org/10.1007/s13738-018-1347-6
58. S.K. Nayak et al., Effect of substitution on molecular conformation and packing features in a series of aryl substituted ethyl-6-methyl-4-phenyl-2-thioxo-1,2,3,4-tetrahydropyrimidine-5-carboxylates. CrystEngComm **12**(4), 1205–1216 (2010). https://doi.org/10.1039/B919648J
59. S. Chitra et al., 5-Acetyl-4-(4-methoxyphenyl)-6-methyl-3, 4-dihydropyrimidin-2 (1H)-one. Acta Crystallogr. Sect. E: Struct. Rep. Online **65**(1), o23–o23 (2009). https://doi.org/10.1107/S1600536808040270
60. D.T. Cremer, J.A. Pople, General definition of ring puckering coordinates. J. Am. Chem. Soc. **97**(6), 1354–1358 (1975). https://doi.org/10.1021/ja00839a011
61. O.V. Shishkin et al., Molecular structure and conformation flexibility of 2-oxo-and 2-thioxo-1,2,3,4-tetrahydropyrimidines and their derivatives. Russ. Chem. Bull. **46**(11), 1838–1843 (1997). https://doi.org/10.1007/BF02503768
62. H. Yuvaraj et al., Ethyl 4-(3-bromophenyl)-6-methyl-2-oxo-1, 2, 3, 4-tetrahydropyrimidine-5-carboxylate. Acta Crystallogr. Sect. E: Struct. Rep. Online **66**(12), o3325–o3325 (2010). https://doi.org/10.1107/S1600536810049019
63. S. Bharanidharan et al., Crystal structure of ethyl 6-(chloromethyl)-4-(4-chlorophenyl)-2-oxo-1,2,3,4-tetrahydropyrimidine-5-carboxylate. Acta Crystallogr. Sect. E: Struct. Rep. Online **70**(11), o1185–o1186 (2014). https://doi.org/10.1107/S1600536814023046
64. H. Kargar et al., Synthesis, spectral characterization, SC-XRD, HSA, DFT and catalytic activity of novel dioxovanadium (V)

complex with aminobenzohydrazone Schiff base ligand: an experimental and theoretical approach. Inorg. Chim. Acta **526**, 120535 (2021). https://doi.org/10.1016/j.ica.2021.120535
65. H. Kargar et al., Zn(II) complexes containing O, N, N, O-donor Schiff base ligands: synthesis, crystal structures, spectral investigations, biological activities, theoretical calculations and substitution effect on structures. J. Coord. Chem. **74**(16), 2720–2740 (2021). https://doi.org/10.1080/00958972.2021.1990271
66. H. Kargar et al., Synthesis, spectral characterization, SC-XRD, HSA, DFT and catalytic activity of a dioxidomolybdenum complex with aminosalicyl-hydrazone Schiff base ligand: an experimental and theoretical approach. Polyhedron **208**, 115428 (2021). https://doi.org/10.1016/j.poly.2021.115428
67. H. Kargar et al., Titanium(IV) complex containing ONO-tridentate Schiff base ligand: synthesis, crystal structure determination, Hirshfeld surface analysis, spectral characterization, theoretical and computational studies. J. Mol. Struct. **1241**, 130653 (2021). https://doi.org/10.1016/j.molstruc.2021.130653
68. K. Hadi et al., Synthesis, characterization, crystal structures, Hirshfeld surface analysis, DFT computational studies and catalytic activity of novel oxovanadium and dioxomolybdenum complexes with ONO tridentate Schiff base ligand. Polyhedron **202**, 115194 (2021). https://doi.org/10.1016/j.poly.2021.115194
69. M.J. Turner et al., Visualisation and characterisation of voids in crystalline materials. CrystEngComm **13**(6), 1804–1813 (2011). https://doi.org/10.1039/C0CE00683A
70. H. Kargar et al., Synthesis, crystal structure determination, Hirshfeld surface analysis, spectral characterization, theoretical and computational studies of titanium (IV) Schiff base complex. J. Coord. Chem. **74**(16), 2682–2700 (2021). https://doi.org/10.1080/00958972.2021.1972984
71. H. Kargar et al., Experimental and theoretical studies of new dioxomolybdenum complex: synthesis, characterization and application as an efficient homogeneous catalyst for the selective sulfoxidation. Inorg. Chim. Acta **527**, 120568 (2021). https://doi.org/10.1016/j.ica.2021.120568
72. M. Fallah-Mehrjardi et al., Symmetrical Pd(II) and Ni(II) Schiff base complexes: synthesis, crystal structure determination, spectral characterization, and theoretical studies. J. Mol. Struct. **1251**, 132037 (2022). https://doi.org/10.1016/j.molstruc.2021.132037
73. H. Kargar et al., Synthesis, characterization, SC-XRD, HSA and DFT study of a novel copper(I) iodide complex with 2-(thiophen-2-yl)-4,5-dihydro-1H-imidazole ligand: an experimental and theoretical approach. J. Mol. Struct. **1253**, 132264 (2022). https://doi.org/10.1016/j.molstruc.2021.132264
74. H. Kargar et al., Novel copper(II) and zinc(II) complexes of halogenated bidentate N,O-donor Schiff base ligands: synthesis, characterization, crystal structures, DNA binding, molecular docking, DFT and TD-DFT computational studies. Inorg. Chim. Acta **514**, 120004 (2021). https://doi.org/10.1016/j.ica.2020.120004
75. H. Kargar et al., Synthesis, characterization, crystal structures, DFT, TD-DFT, molecular docking and DNA binding studies of novel copper (II) and zinc (II) complexes bearing halogenated bidentate N,O-donor Schiff base ligands. Polyhedron **195**, 114988 (2021). https://doi.org/10.1016/j.poly.2020.114988